Journal of Biomechanics 145 (2022) 111362

Contents lists available at ScienceDirect

Journal of Biomechanics

journal homepage: www.elsevier.com/locate/jbiomech

Fluid-sensitive migration mechanisms predict association between metastasis and high interstitial fluid pressure in pancreatic cancer

Geir Nævdal [a], Einar K. Rofstad [b], Kjetil Søreide [c,d,e], Steinar Evje [f,*]

[a] NORCE Norwegian Research Centre AS, Bergen, Norway
[b] Department of Radiation Biology, Institute for Cancer Research, Oslo University Hospital, Oslo, Norway
[c] Department of Gastrointestinal Surgery, Stavanger University Hospital, Stavanger, Norway
[d] Department of Clinical Medicine, University of Bergen, Norway
[e] Gastrointestinal Translational Research Group, Laboratory for Molecular medicine, Stavanger University Hospital, Norway
[f] Faculty of Science and Technology, Group of Computational Engineering, University of Stavanger, Norway

ARTICLE INFO

Keywords:
Cell-migration
Interstitial fluid pressure
Autologous chemotaxis
Metastasis
Pancreatic cancer
Mathematical modeling

ABSTRACT

A remarkable feature in pancreatic cancer is the propensity to metastasize early, even for small, early stage cancers. We use a computer-based pancreatic model to simulate tumor progression behavior where fluid-sensitive migration mechanisms are accounted for as a plausible driver for metastasis. The model has been trained to comply with in vitro results to determine input parameters that characterize the migration mechanisms. To mimic previously studied preclinical xenografts we run the computer model informed with an ensemble of stochastic-generated realizations of unknown parameters related to tumor microenvironment only constrained such that pathological realistic values for interstitial fluid pressure (IFP) are obtained. The in silico model suggests the occurrence of a steady production of small clusters of cancer cells that detach from the primary tumor and form isolated islands and thereby creates a natural prerequisite for a strong invasion into the lymph nodes and venous system. The model predicts that this behavior is associated with high interstitial fluid pressure (IFP), consistent with published experimental findings. The continuum-based model is the first to explain published results for preclinical models which have reported associations between high IFP and high metastatic propensity and thereby serves to shed light on possible mechanisms behind the clinical aggressiveness of pancreatic cancer.

1. Introduction

Pancreatic cancer is one of the deadliest of all solid organ malignancies, with <8% overall 5-year survival even after surgical resection. Almost 90% of all pancreatic malignancies are pancreatic ductal adenocarcinomas (PDAC) (Leinonen et al., 2017). Most PDACs are resistant to chemotherapy and radiation treatment (Castellanos et al., 2011) and surgery is the only treatment modality that may result in cure (Winter et al., 2012). A majority (almost 80%) of patients with pancreatic cancer have locally advanced disease or distant metastases at the time of diagnosis and the predominant presentation at an advanced stage clearly explains why pancreatic cancers are so deadly (Siegel et al., 2018). A remarkable feature in pancreatic cancer is the propensity to metastasize early, even for small, early stage cancers (Ansari et al., 2017; Hur et al., 2016). A further contributor to poor cancer biology is the invasion of small veins that occurs remarkably common in pancreatic cancer and is a relatively unique feature of PDAC compared with cancers of other organs. Venous invasion is identifiable in two-thirds of surgically resected pancreatic cancers (Noe et al., 2018). In addition, the microenvironment of PDACs is characterized by an abundant desmoplastic stroma that may occupy up to 80% of the tumor volume (Whatcott et al., 2015; Feig et al., 2012). The PDAC stroma consists of a dynamic assortment of extracellular matrix components including fibronectin, collagen, proteoglycans, and hyaluronic acid, nonmalignant cells including fibroblasts, endothelial cells, and immune cells, and soluble proteins such as growth factors and cytokines (Feig et al., 2012). Of clinical relevance, the PDAC stroma represents a physical barrier to the delivery of chemotherapeutic agents and simultaneously supports tumor growth and promotes metastatic dissemination. The dense desmoplastic stroma has been suggested to be a determinant of the aggressive metastatic growth (Whatcott et al., 2015; Feig et al., 2012). The development of an abundant stroma during tumor growth distorts the architecture of the normal pancreas, resulting in an abnormal configuration of blood vessels and lymphatics in PDACs (Neesse et al., 2011; Andersen et al., 2017; Hansem et al., 2019). Geometric

* Corresponding author.
E-mail address: steinar.evje@uis.no (S. Evje).

https://doi.org/10.1016/j.jbiomech.2022.111362
Accepted 26 October 2022
Available online 29 October 2022

Table 1
Model variables.

Variable	Description	Source
α_c, α_w	Volume fraction of cell and fluid	Eq. $(S1)_{1,2}$
S_c	Cell growth/death	Eq. $(S1)_{1,2}$
$\mathbf{u}_c$, $\mathbf{u}_w$	Interstitial cell and fluid velocity	Eq. $(S1)_{3,4}$
P_w, ΔP_{cw}, Λ_C	IFP, cell–cell stress, chemotaxis stress	Eq. $(S1)_3$
$\hat{\xi}_c$, $\hat{\xi}_w$, $\hat{\xi}_{cw}$	Cell-ECM, fluid-ECM, cell-fluid interaction coefficients	Eq. $(S1)_{3,4}$ and (S2)
Q_v, Q_l	Fluid between interstitium and vasculature, lymphatics	Eq. (S4) and (S5)
T_v, T_l	Conductivity of vascular, lymphatic vessel wall	Eq. (S4) and (S5)
$\widetilde{P}_v^*$, $\widetilde{P}_l^*$	Effective vascular pressure, lymphatic pressure	Eq. (S4) and (S5)
ρ, G, C	ECM component, protease, chemokine	Eq. $(S1)_{5-7}$

resistance to blood flow is high in microvascular networks showing high fractions of low-diameter vessels, resulting in elevated microvascular pressure (Stylianopoulos et al., 2018). Preclinical and clinical investigations have revealed that PDACs may show highly elevated interstitial fluid pressure (IFP) (Chauhan et al., 2014; DuFort et al., 2016) as well as high fractions of hypoxic tissue (Dhani et al., 2015). Intertwining in vivo and in vitro data and in silico models are essential to overcome intrinsic challenges associated with a complex system like PDAC (Jackson et al., 2014; Yankeelov et al., 2015; Zhang et al., 2017; Jarrett et al., 2021). In this work we use an in silico PDAC model to deal with the interplay between data from in vitro experiments based on microfluidic systems and data from preclinical models and clinical patient-derived observations. The proposed mathematical model builds on a previously derived computer model (Waldeland and Evje, 2018; Evje and Waldeland, 2019) that has been trained with data from in vitro experiments (Shields et al., 2007; Shieh et al., 2011; Polacheck et al., 2011). These experimental studies have focused on detecting finer details of fluid-driven migration mechanisms motivated by the fact that many solid tumors are associated with elevated interstitial fluid pressure (IFP) (Netti et al., 2003; Stylianopoulos et al., 2018; Andreozzi et al., 2019; Nia et al., 2020; Follain et al., 2020; Zhou et al., 2021). In addition, the in silico PDAC model is informed with input data as reported from the study of preclinical models of human PDAC (Andersen et al., 2017) with focus on various aspects of the tumor microenvironment (TME). We aim at using the model to shed light on the questions: Why is lymphatic and venous invasion so common in pancreatic cancer? Which associations can be found between metastatic propensity and characteristics of the TME? A natural presumption for having a large and aggressive invasion of cancer cells to the lymphatics and the venous system in the peritumoral region is that there are small clusters of tumor cells that escape from the primary tumor. If the pancreatic cancer cells are encoded with well-tuned migration mechanisms promoting this behavior, this suggests an explanation why it is so difficult to detect metastatic spreading, even for small tumors (Hruban et al., 2019).

2. Methods

The mathematical model builds on our recently published framework (Waldeland and Evje, 2018; Evje and Waldeland, 2019; Waldeland et al., 2021). The baseline parameters of the model are summarized in Table S1–S4 (Supporting Information). Description of model equations, methodology, and limitations can be found in Supporting Information. A main novelty of the current paper is to adapt the model to a setting which is relevant for preclinical and clinical data. New elements that must be addressed are: (i) Represent the unknown stochastic intratumoral vasculature as well as the collecting peritumoral lymphatic network in an appropriate form; (ii) Show that the two competing fluid-sensitive migration mechanisms, when exposed to a realistic fluid velocity field, have the ability to create aggressive behavior; (iii) Verify that this aggressive behavior, in terms of number of isolated islands that are formed, in fact are correlated to higher IFP.

3. Results

Recent research has highlighted the potential important role played by fluid flow as a driver for metastatic dissemination (Nia et al., 2020; Follain et al., 2020; Zhou et al., 2021). We formulate the computer model as simple as possible in terms of number of different cells (cancer cells, fibroblasts and other stromal cells, immune cells, etc.), different chemical components (chemokines, cytokines, proteases, growth factors, etc.), and stromal components (ECM components). Main variables that are used in the model are given in Table 1. The starting point for model simulations is a non-metastatic, coherent primary solid tumor (see Fig. 1A, left) where the pancreatic cancer cells are armed with two fluid-sensitive migration mechanisms (Shields et al., 2007; Shieh et al., 2011; Polacheck et al., 2011). Faced with the fact that not much details are known regarding the TME, we run the in silico PDAC model informed with an ensemble of stochastic generated realizations of parameters that characterize features of the physicochemical microenvironment (Waldeland et al., 2021). The following aspects of the TME is varied:

(i) Amount of produced fluid due to varying density and position of leaky microvascular vessels as expressed through $T_v(\mathbf{x})$, see Eq. (S4) and Eq. (S8) in Supporting Information, and high internal pressure $\widetilde{P}_v^*$ (which is kept constant) reflecting high resistance to blood flow. A typical example of $T_v(\mathbf{x})$ is visualized in Fig. 1A (middle);

(ii) Amount of fluid collected through the peritumoral lymphatics and venous system as represented by $T_l(\mathbf{x})$, see Eq. (S5) and Eq. (S9) in Supporting Information. A typical example of $T_l(\mathbf{x})$ is shown in Fig. 1A (right);

(iii) density of the PDAC stroma expressed in terms of its hydraulic conductivity through $\hat{\xi}_w$, see Eq. $(S1)_4$, Eq. (S2), and Eq. (S3) combined with Eq. (S7) in Supporting Information.

Armed with the simulated ensemble of in silico tumors, we analyze these computer generated data and search for associations between metastatic propensity and features of the physicochemical microenvironment. Model assumptions are:

(i) We assume an aggressive cell line whose aggressiveness is characterized by the choice of parameters that determine the strength of the first and last term of Eq. (S6) associated with the upstream and downstream migration (Waldeland and Evje, 2018; Evje and Waldeland, 2019). We refer to Supporting Information Table (S3) and Table (S4) for values.

(ii) We consider a domain of size $1\ \text{cm} \times 1\ \text{cm}$ and assume characteristic length $L^* = 1$ cm and characteristic time $T^* = 10^4$ s (Supporting Information Table (S1)) and consider a simulation period of $T = 25$ (dimensionless) which amounts to approximately 69 h. We consider an ensemble of 50 randomly generated realizations of $\hat{k}_w$ (dimensionless), $T_v(\mathbf{x})$, and $T_l(\mathbf{x})$ ($[\text{Pa s}]^{-1}$) as described, respectively, in Eq. (S7), (S8), and (S9) (Supporting Information).

(iii) In the preclinical study (Andersen et al., 2017), metastatic propensity is quantified by exploring the peritumoral lymph nodes and measuring their length. Metastatic propensity in the context of the in silico model is measured by computing the averaged number of isolated islands of tumor cells which have been formed during the time period $[0, T]$. More precisely, we introduce the set E_ϵ that identifies the

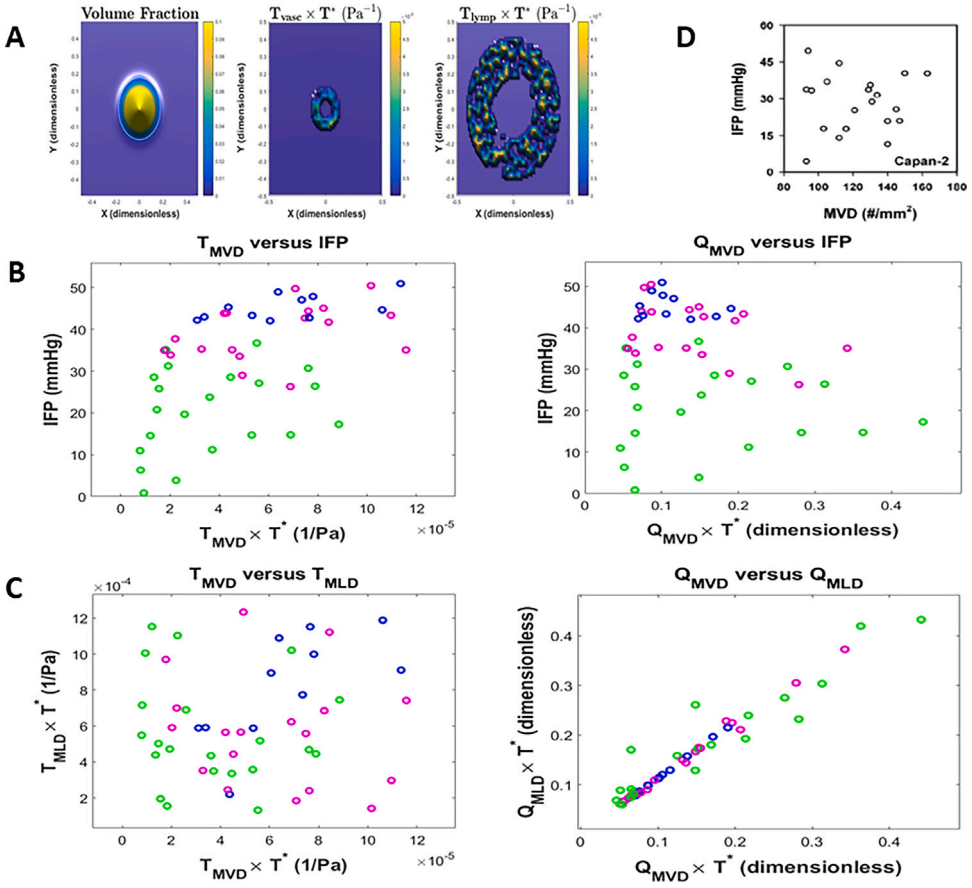

Fig. 1. The physicochemical microenvironment (1 cm × 1 cm) of the in silico PDAC model versus preclinical data. **A**, Primary tumor before simulation starts (left), example of $T_v(\mathbf{x})$ generated from Eq. (S2) in Supplementary Data characterizing the intratumoral microvascular network (middle), and $T_l(\mathbf{x})$ generated from Eq. (S3) in Supplementary Data describing the peritumoral lymphatic network (right). **B**, Plot of interstitial fluid pressure (IFP) vs. microvascular density through T_{MVD} (left) and Q_{MVD} (right). **C**, Plot of T_{MVD} vs. T_{MLD} (left) and Q_{MVD} vs. Q_{MLD} (right). Green circle = non-metastatic growth ($n = 0$). Pink circle = medium metastatic propensity ($1 \le n \le 4$). Blue circle = high metastatic propensity ($n \ge 5$). **D**. (For interpretation of the references to colour in this figure legend, the reader is referred to the web version of this article.)
Source: Data from PDAC preclinical model reproduced from Andersen et al. (2017) reflecting microvascular density (MVD) vs. IFP.

connected regions with a cell volume fraction larger than or equal to a lower limit ϵ

$$E_\epsilon(\mathbf{x}, t) = \{\mathbf{x} \in \Omega \mid \alpha_c(\mathbf{x}, t) \ge \epsilon\}, \tag{1}$$

where we choose $\epsilon \in [0.005, 0.025]$. For the simulation results presented below, we have set $\epsilon = 0.011$. From $E_{0.011}(\mathbf{x}, t)$, we count the number of isolated islands $N(t)$ at any time t. Finally, we take the average of $N(t)$ over $[0, T]$

$$n \approx \overline{N} = \frac{1}{T}\int_0^T N(s)\, ds \tag{2}$$

which gives the averaged number of isolated islands $\overline{N}$. This number is rounded off to its nearest integer $n \approx \overline{N}$ and used as a metric to measure metastatic propensity. We have grouped the degree of aggressiveness into the following categories (motivated by Andersen et al. (2017)): $n = 0$ (non-metastatic), $1 \le n \le 4$ (medium metastases), and $n \ge 5$ (strong metastases).

(iv) As a measure of the intratumoral density of the microvascular system (MVD), we use the following quantities Q_{MVD} (s^{-1}) and T_{MVD} ([Pa s]$^{-1}$) extracted from the computer model:

$$\begin{aligned} Q_{MVD} &= \int_{\Omega_{vasc}} Q_v(\mathbf{x})\, d\mathbf{x} = \int_{\Omega_{vasc}} T_v(\mathbf{x})(\widetilde{P}_v^* - P_w)\, d\mathbf{x}, \\ T_{MVD} &= \int_{\Omega_{vasc}} T_v(\mathbf{x})\, d\mathbf{x}. \end{aligned} \tag{3}$$

Q_{MVD} represents the total amount of fluid that is produced from the intratumoral leaky vascular system. We note that Q_{MVD} is influenced by IFP P_w which in turn is sensitive to whether the ECM is dense or sparse. In contrast, T_{MVD} is more directly related to the density of the microvascular network. Similarly, we introduce Q_{MLD} and T_{MLD} given by

$$\begin{aligned} Q_{MLD} &= \int_{\Omega_{lymp}} Q_l(\mathbf{x})\, d\mathbf{x} = \int_{\Omega_{lymp}} T_l(\mathbf{x})(P_w - \widetilde{P}_l^*)\, d\mathbf{x}, \\ T_{MLD} &= \int_{\Omega_{lymp}} T_l(\mathbf{x})\, d\mathbf{x} \end{aligned} \tag{4}$$

to characterize the lymphatic network and its ability to drain interstitial fluid in the peritumoral region.

(v) We use the variable $\hat{k}_w$ to divide the ECM into three different categories: (i) sparse, which amounts to $1 \le \hat{k}_w \le 11$; (ii) intermediate, which amounts to $11 < \hat{k}_w < 19$; (iii) dense, which amounts to $19 \le \hat{k}_w \le 30$. In other words, we use the level of resistance force felt by the interstitial fluid as it flows as a measure of the density of ECM (Wu et al., 2013; Waldeland et al., 2021).

Associations between metastatic behavior and the physicochemical microenvironment were searched for by comparing maximal IFP ($P_{max} = \max_{\Omega_{vasc}} P_w$), Q_{MVD} (or T_{MVD}) and Q_{MLD} (or T_{MLD}) as given by (3) and (4). The computed values were related to the metastatic status as expressed by #n of isolated clusters of tumor cells (island) to mimic the study of preclinical models of human PDAC (Andersen et al., 2017). The underlying assumption is that isolated islands is an indicator of the tendency to generate dissemination of tumor cells to peritumoral lymphatics (Onozato et al., 2013). For statistical analysis of the in silico generated data we rely on the Wilcoxon rank sum test

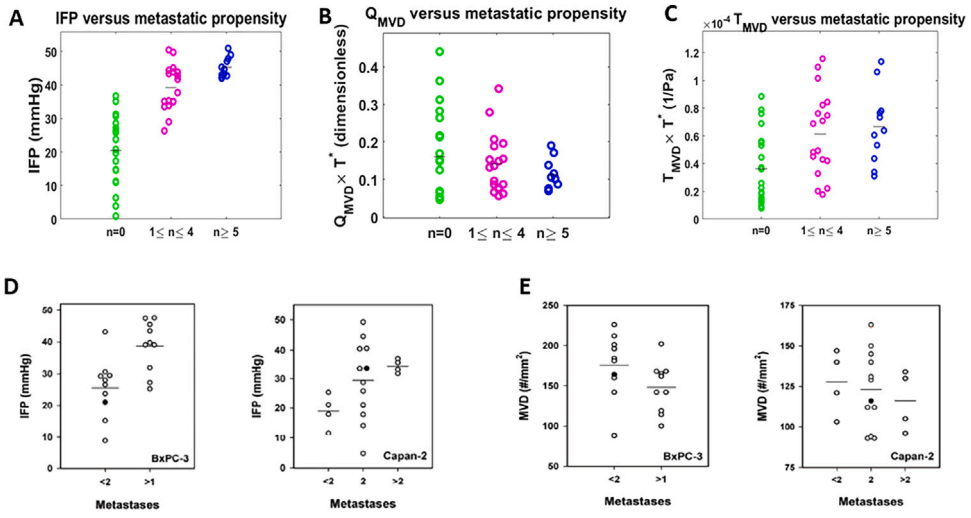

Fig. 2. The metastatic propensity of the in silico PDAC model. **A**, Interstitial fluid pressure (IFP) in tumors with non-metastatic growth ($n = 0$), medium metastatic propensity ($1 \le n \le 4$), and high metastatic propensity ($n \ge 5$.) **B**, Q_{MVD} vs. metastatic propensity. **C**, T_{MVD} vs. metastatic propensity. **D**, Data from two PDAC preclinical models reflecting IFP vs. metastatic propensity (reproduced from Andersen et al. (2017)). **E**, Data from preclinical PDAC models reflecting vascular density (MVD) vs. metastatic propensity. *Source:* Reproduced from Andersen et al. (2017)

(Mann Whitney U Test) as implemented in MATLAB, The MathWorks, Inc., Natick, Massachusetts, United States.

3.1. Model predicts that metastatic propensity is associated with high IFP

The physicochemical tumor microenvironment of the generated in silico tumors differed substantially. We observed that T_{MVD} varied between $1{\cdot}10^{-5}/T^*$ and $12{\cdot}10^{-5}/T^*$, see Fig. 1B (left). We found that IFP varied approximately between 1 and 51 mmHg whereas Q_{MVD} varied between $0.05/T^*$ and $0.44/T^*$, see Fig. 1B (right). For the lymphatic network it was observed that T_{MLD} varied between $1 \cdot 10^{-4}/T^*$ and $12 \cdot 10^{-4}/T^*$ (Fig. 1C, left) whereas Q_{MLD} varied between $0.06/T^*$ and $0.43/T^*$ (Fig. 1C, right). The metastatic level varied between 0 and 12 groups of tumor cells that had detached from the primary tumor and formed isolated islands as computed by (2). In Fig. 1C (left) T_{MVD} and T_{MLD} have been plotted. As expected, there is no correlation between these quantities as they have been generated randomly and independently. Fig. 1B (left) shows that IFP did not correlate with T_{MVD} characterizing the microvascular density (MVD) nor Q_{MVD}, see Fig. 1B (right). This is consistent with the preclinical data shown in Fig. 1D. On the other hand, from Fig. 1C (right), we see that there is a rather clear correlation between Q_{MVD} and Q_{MLD} which characterize, respectively, the amount of fluid that leaks from the vascular system and the amount that is collected in the peritumoral region. This visualizes the fact that the underlying conductivity, through $\hat{k}_w$, is homogeneous and that there is a good balance between fluid produced and collected. Regarding the metastatic propensity the total number of in silico tumors with no detachment, i.e., $n = 0$, was found to be 21, the number with mild (medium) metastasis, i.e., $1 \le n \le 4$, was 18, whereas the number of tumors with strong metastatic propensity ($n \ge 5$) was found to be 11. Fig. 2A shows that the more metastatic-positive (both medium and high) tumors had significantly higher IFP than the non-metastatic ($P = 3 \cdot 10^{-6} < 0.05$ and $P = 5 \cdot 10^{-6} < 0.05$, respectively). This is consistent with preclinical data from (Andersen et al., 2017) shown in Fig. 2D for two different PDAC models. On the other hand, these three different groups did not differ significantly in terms of leaked IF reflected by Q_{MVD} (Fig. 2B) with P-values given by $P = 0.8 > 0.05$ and $P = 0.8 > 0.05$, when comparing non-metastatic group versus medium and high metastatic propensity group, respectively. The corresponding visualization of T_{MVD} (Fig. 2C) also shows behavior similar to preclinical data in Fig. 2E. A finer check of the role of the density of ECM as reflected by the coefficient $\hat{k}_w$ representing the fluid-ECM resistance force, is shown in Fig. 3. We found that 20 of the in silico tumors were in the category sparse ECM, 12 classified as medium ECM, and the remaining 18 classified as dense ECM. For all three categories (sparse is shown in panel A, medium in panel B, dense in panel C) the same correlation is reflected that higher metastatic propensity is associated with high IFP. The P-value in Fig. 3A is $P = 0.0074 < 0.05$ when we compare non-metastatic versus metastatic group. The corresponding P-values in Fig. 3B and C are $P = 0.004 < 0.05$ and $P = 0.0098 < 0.05$, respectively. The case with sparse ECM shown in Fig. 3A reflects a situation with many instances of non-metastatic propensity and a large spread in the IFP ranging from 1 to 37 mmHg. For dense ECM shown in Fig. 3C, it is the opposite with many instances of high metastatic propensity and IFP varying from approximately 40 to 52 mmHg. Taken together, the above observations suggest that the metastatic propensity was associated with high IFP but not with high (or low) leakage of fluid through Q_{MVD}. This behavior is similar to what was reported in Andersen et al. (2017) for two preclinical models (Capan-2 and BxPC-3) as shown in Fig. 2D, which may be compared to Fig. 2A for the in silico model. The in silico model also suggests that high IFP combined with denser ECM (Fig. 3B and C combined) is a more certain indication of high metastatic propensity than when ECM is sparse (Fig. 3A).

Having looked at the ensemble behavior of the in silico PDAC models, we now turn to more detailed simulations of selected samples from the total ensemble of 50 PDAC models. The only preference used in this selection is that they demonstrate clearly different types of tumor progression behavior, i.e., metastatic versus non-metastatic.

3.2. Sparse ECM is associated with less metastatic propensity

We take a closer look at the tumor progression pattern predicted by the in silico PDAC model. We focus on two of the instances shown in Fig. 3A which correspond to tumors with sparse ECM. We are interested to see under what circumstances metastatic behavior may evolve. We select case #23 for that purpose. The simulation result is shown in Fig. 4 at time $T = 25$. We find that the number of isolated clusters of tumor cells that form vary between 0 and 7 with an average equal to $n = 4$, see Fig. 4B. The invasive front is heterogeneous and the periphery of the primary tumor contains finger-like parts (Fig. 4A). The cell velocity associated with the isolated clusters is relatively high (Fig. 4C) and seems correlated to the accumulated high chemokine concentration in the peritumoral region (Fig. 4E). The interstitial fluid velocity (Fig. 4F)

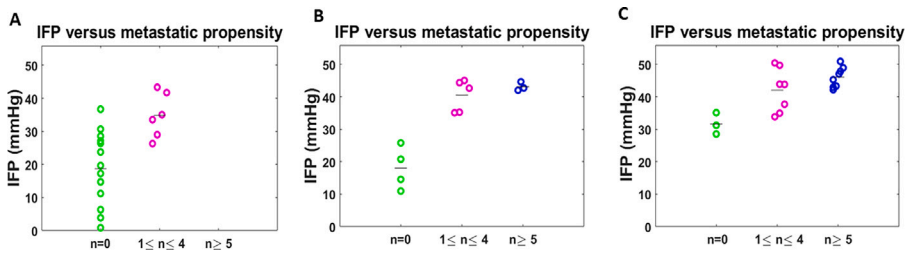

Fig. 3. The metastatic propensity of the in silico PDAC model with varying ECM density. Interstitial fluid pressure (IFP) in tumors with non-metastatic growth ($n = 0$), medium metastatic propensity ($1 \le n \le 4$), and high metastatic propensity ($n \ge 5$.) **A**, Sparse ECM ($1 \le \hat{k}_w \le 11$). **B**, Medium ECM ($11 < \hat{k}_w < 19$). **C**, Dense ECM ($19 \le \hat{k}_w \le 30$).

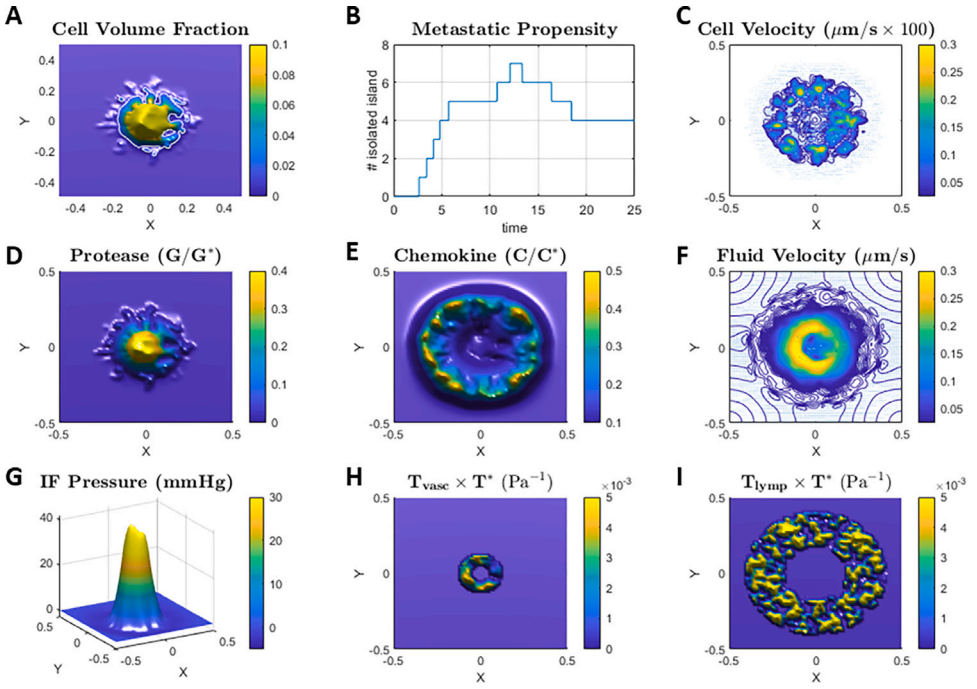

Fig. 4. Sparse ECM with medium metastatic propensity (#23 with $n = 4$) explored in a 1 cm × 1 cm domain. **A**, Cell volume fraction α_c. **B**, Metastatic propensity measured through $N(t)$, i.e., the number of isolated islands, which varies between 0 and 7. **C**, Cell velocity $\mathbf{u}_c$. **D**, Proteases G. **E**, Chemokine C. **F**, Interstitial fluid velocity $\mathbf{u}_w$. **G**, Interstitial fluid pressure P_w. **H**, T_v characterizing the density of leaky blood vessels. **I**, T_l characterizing the density of collecting lymphatics.

is a result of the leaked fluid from the intratumoral vascular network (Fig. 4H) and the collecting lymphatic network (Fig. 4I) and the tissue conductivity through $\hat{k}_w$ (here $\hat{k}_w \approx 10$). The IFP (Fig. 4G) takes a maximal pressure close to 42 mmHg. The main reason for this relatively high IFP for this case with sparse ECM is the high value of T_v shown in Fig. 4H.

Secondly, we illustrate an example, still for the case with sparse ECM, where there is no metastatic behavior, i.e., $n = 0$. We consider case #10 for that purpose. The only difference between this case and the previous is $\hat{k}_w$, T_v, and T_l. The simulation result is shown in Fig. 5. For this case the hydraulic conductivity is slightly higher as $\hat{k}_w \approx 6$ (i.e., less resistance force felt by the fluid). Looking at Fig. 5H we see that the amount of leaky microvascular vessels is considerably lower compared to the previous example in Fig. 4. This gives rise to a lower IFP shown in Fig. 5G (around 29 mmHg). This implies a lower stress from the fluid on the tumor cells that results in a weaker mobilization of the upstream migration mechanism through $\frac{\hat{f}_c(\alpha_c)}{\alpha_c}\mathbf{U}_T$, see discussion of Eq. (S6) in Supporting Information. Panel 5A shows that the resulting invasive front is somewhat irregular but no clusters of cells have been able to detach throughout the simulation period (Fig. 5B).

3.3. Dense ECM increases the metastatic propensity

We focus on the cases with tumor evolution when ECM is dense. As seen in Fig. 3C, when ECM is dense (i.e., $\hat{k}_w$ is high) most of the samples show medium or high metastatic propensity. What is a typical behavior for this group? As a representative example we consider case #30. The simulated result is shown in Fig. 6. The situation seen here strongly contrasts the previous case. We counted up to 16 isolated groups of cancer cells (Fig. 6B) during the simulated period. ECM density is high as represented by $\hat{k}_w \approx 29$. Most strikingly is the high and heterogeneous T_v seen in panel 6H. This results in a high IFP with a maximum close to 50 mmHg (Fig. 6G). This creates a stronger stress from the fluid on the tumor cells that strengthens the upstream migration mechanism which in turn effectively cleaves groups of cells from the primary coherent tumor, as seen in Fig. 6A. Once this aggressive metastatic migration pattern has been established, it will persistently continue and guide new tumor cells from the primary tumor to the lymphatics.

4. Discussion

The in silico PDAC model has confirmed that the combination of autologous chemotaxis (Shieh et al., 2011) and the upstream fluid stress-mediated mechanism (Polacheck et al., 2011) can give rise to metastatic behavior. Elevated IFP will force interstitial fluid to flow from the tumor tissue into the adjacent peritumoral tissues. This fluid flow may transport proteolytic enzymes and chemokines that facilitate tumor cell migration towards lymphatic vessels (Fink et al., 2016;

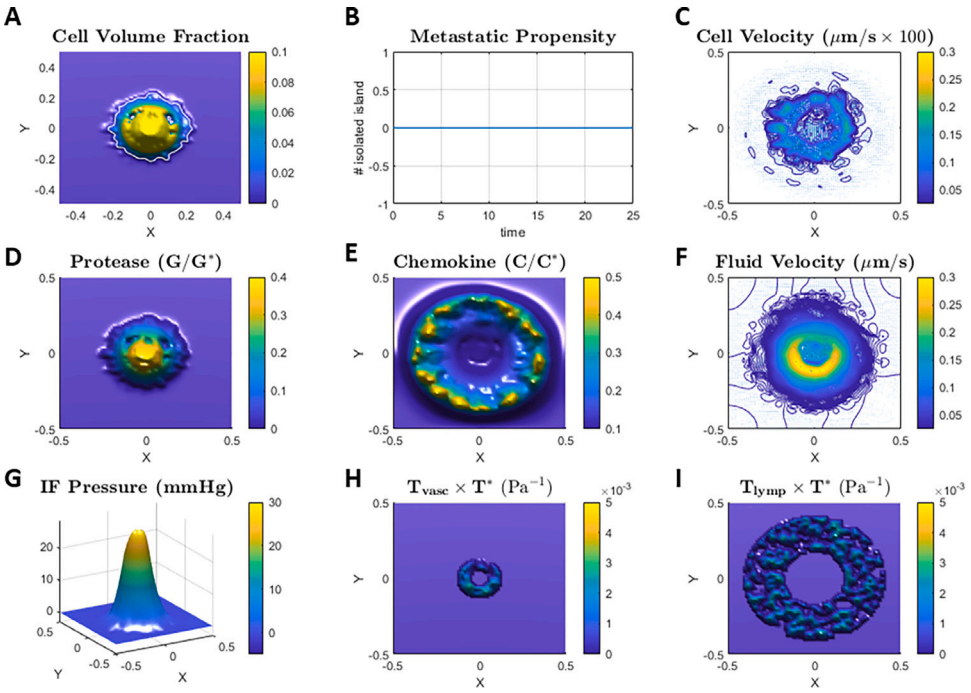

Fig. 5. Sparse ECM with non-metastatic tumor progression (#10 with $n = 0$) explored in a 1 cm × 1 cm domain. **A**, Cell volume fraction α_c. **B**, Metastatic propensity measured through $N(t)$ which is zero throughout the simulation period. **C**, Cell velocity $\mathbf{u}_c$. **D**, Proteases G. **E**, Chemokine C. **F**, Interstitial fluid velocity $\mathbf{u}_w$. **G**, Interstitial fluid pressure P_w. **H**, T_v characterizing the density of leaky blood vessels. **I**, T_l characterizing the density of collecting lymphatics.

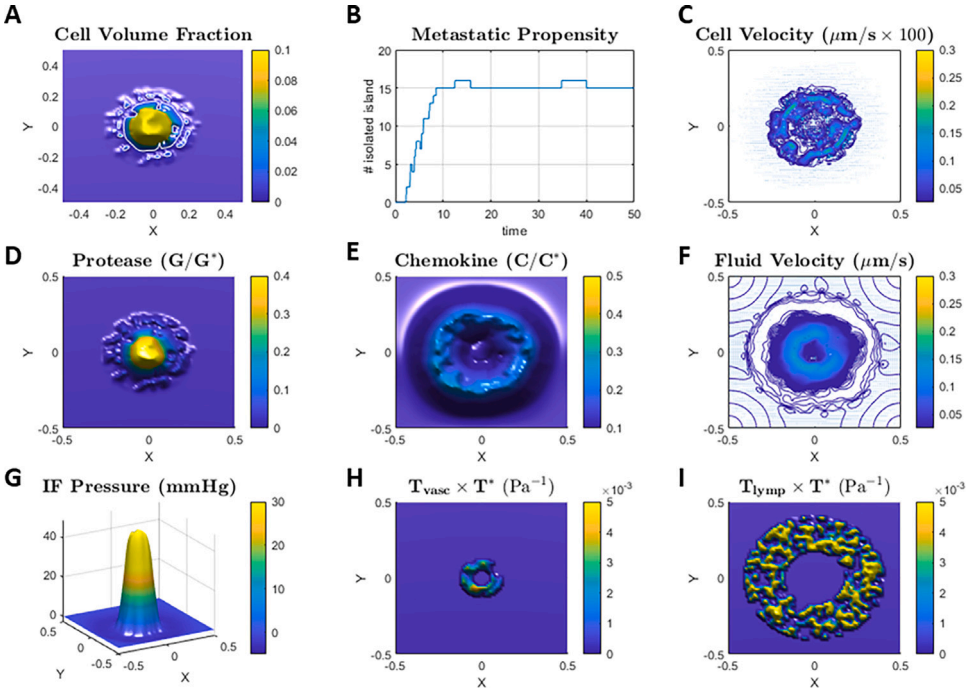

Fig. 6. Dense ECM with high metastatic propensity (#30 with $n = 14$) explored in a 1 cm × 1 cm domain. **A**, Cell volume fraction α_c. **B**, Metastatic propensity measured through $N(t)$. The high level persists throughout the whole simulation period. **C**, Cell velocity $\mathbf{u}_c$. **D**, Proteases G. **E**, Chemokine C. **F**, Interstitial fluid velocity $\mathbf{u}_w$. **G**, Interstitial fluid pressure P_w. **H**, T_v characterizing the density of leaky blood vessels. **I**, T_l characterizing the density of collecting lymphatics.

Andersen et al., 2017; Nia et al., 2020). Combined with the upstream-mediated migration this helps small groups of tumor cells at the periphery to form isolated islands. A major challenge in pancreatic cancer treatment is the presence in lymph nodes of single or small clusters of tumor cells (Fink et al., 2016). The preclinical PDAC model studied in Andersen et al. (2017) showed distinct ductal structures enclosed by an abundant desmoplastic stroma. The stroma was seen as a dense matrix of connective tissue fibers appearing in thick filament bundles, and the majority of blood vessels were located in these bundles. To mimic this situation we generated stochastic fields of T_v, T_l, and $\hat{k}_w$ as input to the in silico PDAC model but constrained within certain ranges to ensure that the resulting IFP was consistent with the findings in Andersen et al. (2017). The results produced by the in silico model with 50 tumors showed a behavior with striking similarities to the

results reported in Andersen et al. (2017) in the following sense: (i) No correlation was found between IFP and amount of leaked fluid from the intratumoral vascular system through T_{MVD} or Q_{MVD} (Fig. 1B). This behavior is also consistent with other studies both in patients with cervix cancer (Milosevic et al., 2001) and in experimental tumors (Lunt et al., 2008). (ii) No clear association was seen between metastatic propensity and amount of leaked fluid from the intratumoral vascular system through Q_{MVD} or T_{MVD} (Fig. 2B and C). (iii) Clear association was observed between high IFP and metastatic propensity in terms of number of generated isolated groups of tumor cells (Fig. 2A).

The in silico PDAC model suggests that high IFP typically is a result of a proper combination of sufficiently high internal vascular pressure $\widetilde{P}_v^*$, production of IF through Q_v, and high $\hat{k}_w$ (density of ECM). The most aggressive tumor cell migration was seen when the density of ECM was high, see Fig. 3B and C where $\hat{k}_w > 11$. The model suggests that this is due to an increase in the stress from the outgoing fluid at the tumor periphery that triggers tumor cells to go upstream where they are more closely packed (see Fig. 6A). This amplifies a detachment mechanism as cancer cells at the tumor margin, where they are sparsely distributed, is under a stronger dominance of the downstream migration where cells move towards higher chemokine concentrations in the peritumoral region close to the lymphatics, see Fig. 6E. In the recent work (Waldeland et al., 2021) we explored a cell-fibroblast-fluid model where the upstream migration was not included. This model did not reflect that invasive and metastatic behavior was correlated to high IFP. A key point in the current cell-fluid model is the relation between $\hat{k}_{cw}$ and $\hat{k}_w$ in Eq. (S3). It suggests that the upstream force through $\hat{k}_{cw}$ is adjusted by the cancer cells to the cell-fluid resistance force $\hat{k}_w$. A denser ECM (i.e., higher $\hat{k}_w$) gives rise to a stronger stress from the fluid on the cancer cells which respond with a stronger upstream force. Previous preclinical studies for melanoma and cervix carcinoma xenografts have shown that high IFP and lymph node metastasis are correlated both in tumors with and without hypoxic regions (Rofstad et al., 2002; Hompland et al., 2012). This suggests that the detachment mechanism demonstrated in this work might represent a general strategy by which cancer cells can create metastatic dissemination. We can easily envision to modify the model to apply it in the context of other solid tumors where fluid flow is thought to play an active role in the tumor progression. Nearby examples include cervic cancer (Hompland et al., 2012), breast cancer (Shieh et al., 2011; Polacheck et al., 2011), melanoma (Rofstad et al., 2002), and brain cancer (Munson et al., 2013; Kingsmore et al., 2016).

Can the proposed in silico PDAC model be relevant for clinical data? The incidence and the site of development of lymph node metastasis depend on the density and structure of the peritumoral lymphatics which may differ in PDAC xenografts versus human PDACs. This may be different from patient to patient, explaining in part the differences observed in preclinical behavior and clinical outcomes. Another aspect is whether there are clinical data available for quantification of ECM density and vascular architecture. This is (currently) only available for assessment in the tissue proper through biopsies or by microscopy of the resected tumor. The latter represents a problem as usually less than 20% of patients with PDAC are resectable at time of diagnosis. Other surrogate measures of ECM density may thus be entertained, currently only available in the experimental setting or by imaging modalities such as CT/MRI or novel techniques of ultrasonography (Li et al., 2019; Wang et al., 2019).

In summary, we have demonstrated a simplest possible computational model, based on sound fluid mechanical and bio-chemical principles on tissue level, that can give a plausible explanation of the association which has been found between metastatic propensity and high IFP for preclinical PDAC models. Future work will seek to enhance the applicability of the model by combining it with robust data assimilation methods for revealing hidden characteristics of TME based on patient-specific type of data, as well as extending it to explore drug delivery scenarios (Stylianopoulos and Jain, 2013; Weis et al., 2015; Dewhirst and Secomb, 2017; d'Esposito et al., 2018).

CRediT authorship contribution statement

Geir Nævdal: Writing – review & editing, Supervision, Methodology. **Einar K. Rofstad:** Writing – original draft, Supervision, Methodology, Data curation, Conceptualization. **Kjetil Søreide:** Writing – original draft, Supervision. **Steinar Evje:** Writing – original draft, Methodology, Investigation, Conceptualization.

Declaration of competing interest

The authors declare that they have no known competing financial interests or personal relationships that could have appeared to influence the work reported in this paper.

Appendix A. Supplementary data

Supplementary material related to this article can be found online at https://doi.org/10.1016/j.jbiomech.2022.111362.

References

Andersen, L.M.K., Wegner, C.S., Simonsen, T.G., Huang, R., Gaustad, J.V., Hauge, A., Galappathi, K., Rofstad, E.K., 2017. Lymph node metastasis and the physicochemical microenvironment of pancreatic ductal adenocarcinoma xenografts. Oncotarget 8, 48060–48074.

Andreozzi, A., Iasiello, M., Netti, P.A., 2019. A thermoporoelastic model for fluid transport in tumour tissues. J. R. Soc. Interface 16 (154).

Ansari, D., Bauden, M., Bergstrom, S., Rylance, R., Marko-Varga, G., Andersson, R., 2017. Relationship between tumour size and outcome in pancreatic ductal adenocarcinoma. Br. J. Surg. 104, 600–607.

Castellanos, E., Berlin, J., Cardin, D.B., 2011. Current treatment options for pancreatic carcinoma. Curr. Oncol. Rep. 13, 195–205.

Chauhan, V.P., Boucher, Y., Ferrone, C.R., Roberge, S., Martin, J.D., Stylianopoulos, T., Bardeesy, N., DePinho, R.A., Padera, T.P., Munn, L.L., Jain, R.K., 2014. Compression of pancreatic tumor blood vessels by hyaluronan is caused by solid stress and not interstitial fluid pressure. Cancer Cell 26, 14–15.

d'Esposito, A., Sweeney, P.W., Ali, M., Saleh, M., Ramasawmy, R., Roberts, TA, Agliardi, G, Desjardins, A., Lythgoe, M.F., Pedley, R.B., Shipley, R., Walker-Samuel, S., 2018. Computational fluid dynamics with imaging of cleared tissue and of in vivo perfusion predicts drug uptake and treatment responses in tumours. Nat. Biomed. Eng. 2, 773–787.

Dewhirst, M., Secomb, T.W., 2017. Transport of drugs from blood vessels to tumour tissue. Nat. Rev. Cancer 17, 738–750.

Dhani, N., Fyles, A., Hedley, D., Milosevic, M., 2015. The clinical significance of hypoxia in human cancers. Semin. Nucl. Med. 45, 110–121.

DuFort, C.C., DelGiorno, K.E., Carlson, M.A., et al., 2016. Interstitial pressure in pancreatic ductal adenocarcinoma is dominated by a gel-fluid phase. Biophys. J. 110, 2106–2119.

Evje, S., Waldeland, J.O., 2019. How tumor cells can make use of interstitial fluid flow in a strategy for metastasis. Cell. Mol. Bioeng. 12, 227–254.

Feig, C., Gopinathan, A., Neesse, A., Chan, D.S., Cook, N., Tuveson, D.A., 2012. The pancreas cancer microenvironment. Clin. Cancer Res. 18, 4266–4276.

Fink, D.M., Steele, M.M., Hollingsworth, M.A., 2016. The lymphatic system and pancreatic cancer. Cancer Lett. 381, 217–236.

Follain, G., Herrmann, D., Harlepp, S., Hyenne, V., Osmani, N., Warren, S.C., Timpson, P., Goetz, J.G., 2020. Fluids and their mechanics in tumour transit: shaping metastasis. Nat. Rev. Cancer 20, 107–124.

Hansem, L.M.K., Huang, R., Wegner, C.S., Simonsen, T.G., Gaustad, J.V., Hauge, A., Rofstad, E.K., 2019. Intratumor heterogeneity in interstitial fluid pressure in cervical and pancreatic carcinoma xenografts. Transl. Oncol. 12, 1079–1085.

Hompland, T., Ellingsen, C., Øvrebø, K.M., Rofstad, E.K., 2012. Interstitial fluid pressure and associated lymph node metastasis revealed in tumors by dynamic contrast-enhanced MRI. Cancer Res. 72, 4899–4908.

Hruban, R.H., Gaida, M.M., Thompson, E., Hong, S.M., Noe, M., Brosens, L.A., Jongepier, M., Offerhaus, G.J.A., Wood, L.D., 2019. Why is pancreatic cancer so deadly? The pathologist's view. J. Pathol. 248, 131–141.

Hur, C., Tramontano, A.C., Dowling, E.C., Brooks, G.A., Jeon, A., Brugge, W.R., Gazelle, G.S., Kong, C.Y., Pandharipande, P.V., 2016. Early pancreatic ductal adenocarcinoma survival is dependent on size: positive implications for future targeted screening. Pancreas 45, 1062–1066.

Jackson, T., Komarova, N., Swanson, K., 2014. Mathematical oncology: Using mathematics to enable cancer discoveries. Am. Math. Month. 121, 840–856.

Jarrett, A.M., Kazerouni, A.S., Wu, C., Virostko, J., Yankeelov, T.E., et al., 2021. Quantitative magnetic resonance imaging and tumor forecasting of breast cancer patients in the community setting. Nat. Prot. 16, 5309–5338.

Kingsmore, K.M., Logsdon, D.K., Floyd, D.H., Peirce, S.M., Purow, B.W., Munson, J.M., 2016. Interstitial flow differentially increases patient-derived glioblastoma stem cell invasion via CXCR4, CXCL12, and CD44-mediated mechanisms. Integr. Biol. 8, 1246.

Leinonen, M.K., Miettinen, J., Heikkinen, S., Pitkaniemi, J., Malila, N., 2017. Quality measures of the population-based finnish cancer registry indicate sound data quality for solid malignant tumours. Eur. J. Cancer 77, 31–39.

Li, J., Zormpas-Petridis, K., Boult, J.K.R., Reeves, E.L., et al., 2019. Investigating the contribution of collagen to the tumor biomechanical phenotype with noninvasive magnetic resonance elastography. Cancer Res. 79, 5874–5883.

Lunt, S.J., Kalliomaki, T.M., Brown, A., Yang, V.X., Milosevic, M., Hill, R.P., 2008. Interstitial fluid pressure, vascularity and metastasis in ectopic, orthotopic and spontaneous tumours. BMC Cancer 8, 2.

Milosevic, M., Fyles, A., Hedley, D., Pintilie, M., Levin, W., Manchul, L., Hill, R., 2001. Interstitial fluid pressure predicts survival in patients with cervix cancer independent of clinical prognostic factors and tumor oxygen measurements. Cancer Res. 61, 6400–6405.

Munson, Jennifer M., Bellamkonda, Ravi V., Swartz, Melody A., 2013. Interstitial flow in a 3D microenvironment increases glioma invasion by a CXCR4-dependent mechanism. Cancer Res. 73 (5), 1536–1546.

Neesse, A., Michl, P., Frese, K.K., Feig, C., Cook, N., Jacobetz, M.A., Lolkema, M.P., Buchholz, M., Olive, K.P., Gress, T.M., Tuveson, D.A., 2011. Stromal biology and therapy in pancreatic cancer. Gut 60, 861–868.

Netti, P.A., Travascio, F., Jain, R.K., 2003. Coupled macromolecular transport and gel mechanics: poroviscoelastic approach. AlChE J. 49, 1580–1596.

Nia, H.T., Munn, L.L., Jain, R.K., 2020. Physical traits of cancer. Science 370.

Noe, M., Rezaee, N., et al., 2018. Immunolabeling of cleared human pancreata provides insights into three-dimensional pancreatic anatomy and pathology. Am. J. Pathol. 188, 1530–1535.

Onozato, M.L., et al., 2013. Tumor islands in resected early stage lung adenocarcinomas are associated with unique clinicopathological and molecular characteristics and worse prognosis. Am. J. Surg. Pathol. 37, 287–294.

Polacheck, W.J., Charest, J.L., Kamm, R.D., 2011. Interstitial flow influences direction of tumor cell migration through competing mechanisms. Proc. Natl. Acad. Sci. USA 108, 11115–11120.

Rofstad, E.K., Tunheim, S.H., Mathiesen, B., Graff, B.A., Halsør, E.F., Nilsen, K., Galappathi, K., 2002. Pulmonary and lymph node metastasis is associated with primary tumor interstitial fluid pressure in human melanoma xenografts. Cancer Res. 62, 661–664.

Shieh, A.C., Rozansky, H.A., Hinz, B., Swartz, M.A., 2011. Tumor cell invasion is promoted by interstitial flow-induced matrix priming by stromal fibroblasts. Cancer Res. 71, 790–800.

Shields, J.D., Fleury, M.E., Yong, C., Tomei, A.A., Randolph, G.J., Swartz, M.A., 2007. Autologous chemotaxis as a mechanism of tumor cell homing to lymphatics via interstitial flow and autocrine CCR7 signaling. Cancer Cell 11, 526–538.

Siegel, R.L., Miller, K.D., A., Jemal, 2018. Cancer statistics. CA Cancer J. Clin. 68, 7–30.

Stylianopoulos, T., Jain, R.K., 2013. Combining two strategies to improve perfusion and drug delivery in solid tumors. Proc. Natl. Acad. Sci. USA 110, 18632–18637.

Stylianopoulos, T., Munn, L.L., Jain, R.K., 2018. Reengineering the physical microenvironment of tumors to improve drug delivery and efficacy: from mathematical modeling to bench to bedside. Trends Cancer 4, 292–319.

Waldeland, J.O., Evje, S., 2018. Competing tumor cell migration mechanisms caused by interstitial fluid flow. J. Biomech. 81, 22–35.

Waldeland, J.O., Gaustad, J.V., Rofstad, E.K., Evje, S., 2021. In silico investigations of intratumoral heterogeneous interstitial fluid pressure. J. Theoret. Biol. 526, 110787.

Wang, H., Mislati, R., Ahmed, R., Vincent, P., Nwabunwanne, S.F., Gunn, J.R., Pogue, B.W., Doyley, M.M., 2019. Elastography can map the local inverse relationship between shear modulus and drug delivery within the pancreatic ductal adenocarcinoma microenvironment. Clin. Cancer Res. 25, 2136–2143.

Weis, J.A., Miga, M.I., Arlinghaus, L.R., Li, X., Abramson, V., Chakravarthy, A.B., Pendyala, P., Yankeelov, T.E., 2015. Predicting the response of breast cancer to neoadjuvant therapy using a mechanically coupled reaction-diffusion model. Cancer Res. 75, 4697–4707.

Whatcott, C.J., Diep, C.H., Jiang, P., Watanabe, A., LoBello, J., Sima, C., Hostetter, G., Shepard, H.M., Von Hoff, D.D., Han, H., 2015. Desmoplasia in primary tumors and metastatic lesions of pancreatic cancer. Clin. Cancer Res. 21, 3561–3568.

Winter, J.M., Brennan, M.F., Tang, L.H., D'Angelica, M.I., Dematteo, R.P., Fong, Y., Klimstra, D.S., Jarnagin, W.R., Allen, P.F., 2012. Survival after resection of pancreatic adenocarcinoma: results from a single institution over three decades. Ann. Surg. Oncol. 19, 169–175.

Wu, M., Frieboes, H.B., McDougall, S.R.M., Chaplain, M.A.J., Cristini, V., Lowengrub, J., 2013. The effect of interstitial pressure on tumor growth: coupling with the blood and lymphatic vascular systems. J. Theoret. Biol. 320, 131–151.

Yankeelov, T.E., Quaranta, V., Evans, K.J., Rericha, E.C., 2015. Toward a science of tumor forecasting for clinical oncology. Cancer Res. 75, 918–923.

Zhang, J., Cunningham, J.J., Brown, J.S., Gatenby, R.A., 2017. Integrating evolutionary dynamics into treatment of metastatic castrate-resistant prostate cancer. Nature Commun. 8, 1816.

Zhou, H., Lei, P., Padera, T.P., 2021. Progression of metastasis through lymphatic system. Cells 10, 627.